Pion-mass dependence of three-nucleon observables

H.-W. Hammer*

Helmholtz-Institut für Strahlen- und Kernphysik (Theorie), Universität Bonn, D-53115 Bonn, Germany

D.R. Phillips† and L. Platter‡

Department of Physics and Astronomy, Ohio University, Athens, OH 45701, USA

(Dated: February 1, 2008)

Abstract

We use an effective field theory (EFT) which contains only short-range interactions to study the dependence of a variety of three-nucleon observables on the pion mass. The pion-mass dependence of input quantities in our "pionless" EFT is obtained from a recent chiral EFT calculation. To the order we work at, these quantities are the $^1S_0$ scattering length and effective range, the deuteron binding energy, the $^3S_1$ effective range, and the binding energy of one three-nucleon bound state. The chiral EFT input we use has the inverse $^3S_1$ and $^1S_0$ scattering lengths vanishing at $m_\pi^{crit} =$ 197.8577 MeV. At this "critical" pion mass, the triton has infinitely many excited states with an accumulation point at the three-nucleon threshold. We compute the binding energies of these states up to next-to-next-to-leading order in the pionless EFT and study the convergence pattern of the EFT in the vicinity of the critical pion mass. Furthermore, we use the pionless EFT to predict how doublet and quartet nd scattering lengths depend on m_π in the region between the physical pion mass and $m_\pi = m_\pi^{crit}$.

Keywords: Renormalization group, limit cycle, quantum chromodynamics, effective field theory, universality

*Electronic address: hammer@itkp.uni-bonn.de
†Electronic address: phillips@phy.ohiou.edu
‡Electronic address: lplatter@phy.ohiou.edu

I. INTRODUCTION

The NPLQCD collaboration recently computed NN correlation functions in QCD by using Monte Carlo techniques to evaluate the QCD path integral on a discrete Euclidean space-time lattice [1]. This provided the first calculation of nuclear physics quantities from full QCD: the NN scattering lengths in the $^3\mathrm{S}_1$ and $^1\mathrm{S}_0$ channel. However, the NPLQCD computation was performed at quark masses which are significantly larger than those in the physical world. This leaves us with the challenge of understanding how observables such as the NN scattering lengths depend on parameters of QCD such as m_u and m_d.

This challenge can be addressed using effective field theories (EFTs). EFTs allow the calculation of physical observables as an expansion in a small parameter that is a ratio of physical scales. In this paper, we will discuss two different EFTs. The first describes the low-energy sector of QCD by exploiting QCD's approximate chiral symmetry [2]. This chiral EFT (χEFT) is a powerful tool for analyzing the properties of hadronic systems at low energies in a systematic and model-independent way. It is formulated in an expansion around the chiral limit of QCD which governs low-energy hadron structure and dynamics. In χEFTs, the quark-mass dependence of operators in the effective Lagrangian is included explicitly. Loops also generate non-analytic dependence on the quark mass, but their effects can be computed in a controlled way, since they can be obtained up to a given order in the expansion parameter m_q/Λ_χ, where $\Lambda_\chi \sim m_\rho$ is the scale of chiral symmetry breaking in QCD. Over the past 15 years, considerable progress has been made in understanding the structure of the nuclear force in this framework [3, 4, 5, 6] but some questions regarding the power counting remain [7, 8, 9, 10, 11].

The quark-mass dependence of the chiral nucleon-nucleon (NN) interaction was studied in Refs. [12, 13, 14]. These studies found that the inverse scattering lengths in the $^3\mathrm{S}_1$–$^3\mathrm{D}_1$ and $^1\mathrm{S}_0$ channels may both vanish if one extrapolates away from the physical limit to slightly larger quark masses.[1] Subsequently, it was pointed out that QCD is close to the critical trajectory for an infrared RG limit cycle in the 3-nucleon sector. This led to the conjecture that QCD could be tuned to lie precisely on the critical trajectory through small changes in the up and down quark masses away from their physical values [15].

In the vicinity of this critical trajectory another EFT becomes useful. In this EFT observables are calculated as an expansion in powers of $R/|a|$, where R is the range of the two-body potential, and a is the two-particle scattering length. In nuclear physics this is the "pionless" EFT; EFT($\not\pi$) [3, 16, 17, 18, 19, 20]. EFT($\not\pi$) has been used to compute a number of NN system observables as a function of $R/|a|$ [4, 5]. In this theory nucleons are described as point particles with zero-range interactions whose strengths are adjusted to reproduce the scattering lengths a_t and a_s. The effective ranges r_s, r_t and higher-order terms in the low-energy expansions of the phase shifts are treated as perturbations. Since the spin-singlet and spin-triplet np scattering lengths of $a_s = -23.8$ fm and $a_t = 5.4$ fm are significantly larger than the NN-interaction's range $R \approx 2$ fm, EFT($\not\pi$)'s expansion in $R/|a|$ is a useful tool for analyzing the NN system at energies $\ll 1/(MR^2)$. In fact, the utility of this EFT is not confined to nuclear physics, since systems where $R/|a|$ is a small parameter also occur in atomic, molecular, and particle physics. In the limit that $R/|a| \to 0$

[1] Due to the nuclear tensor force, the $^3\mathrm{S}_1$ and $^3\mathrm{D}_1$ channels are coupled. This mixing is included in the χEFT calculations while it appears as a higher-order effect in the pionless EFT discussed below. For simplicity, we will only refer to the $^3\mathrm{S}_1$ and $^1\mathrm{S}_0$ partial waves in the following.

such systems exhibit "universal" features, which are completely independent of details of the inter-particle potential [21]. The calculations of Refs. [12, 13, 14] suggested that NN systems with a common light-quark mass $m_u = m_d$ chosen to yield $m_\pi \simeq 200$ MeV would be close to this universality limit.

A particularly striking feature of this limit occurs in the three-nucleon system. In the 1970s Efimov showed that if $|a|$ is much larger than the range R of the interaction there are shallow three-body bound states whose number increases logarithmically with $|a|/R$. In the 'resonant limit' $a \to \pm\infty$, there are infinitely many shallow three-body bound states with an accumulation point at the three-body scattering threshold. If the particles are identical bosons, the ratio of the binding energies of successive states rapidly approaches the universal constant $\lambda_0^2 \approx 515$. Efimov also showed that low-energy three-body observables for different values of a are related by a discrete scaling transformation in which $a \to \lambda_0^n a$, where n is an integer, and lengths and energies are scaled by the appropriate powers of λ_0 [22, 23]. The discrete scaling symmetry is the hallmark of an RG limit cycle [24].

The Efimov effect can also occur for fermions with at least three distinct spin or isospin states and therefore applies to nucleons as well. The extension of EFT($\not\pi$) to the three-nucleon system allows a systematization of Efimov's "qualitative" approach to the three-nucleon problem [25]. In EFT($\not\pi$), treatment of the $S_{1/2}$ nd partial-wave requires the inclusion of a three-body force at leading order in the power counting [26]. It is this three-body force (commonly denoted H_0), whose renormalization-group evolution is governed by a limit cycle. Thus, once one piece of three-body data is used to fix the three-body force at a given regularization scale, other three-body observables can be predicted in EFT($\not\pi$). This provides an explanation for correlations observed empirically in the three-nucleon system, e.g. the "Phillips line" correlation between B_3 and the doublet nd scattering length $a_{nd}^{1/2}$.

But the results such as the Phillips line which were discussed in Ref. [26] were only obtained there up to corrections of order $R/|a|$ and kR, where k is the typical momentum of the process under consideration. The corrections to three-nucleon scattering observables linear in $R/|a|$ were considered in Refs. [27, 28]. Efforts to compute $(R/|a|)^2$ and $(kR)^2$-corrections to three-nucleon observables were pursued in Ref. [29]. However, recent work within a reformulation of the equations describing three-nucleon scattering shows that, once one three-body datum is used to fix the leading-order three-nucleon force, the inclusion of corrections up to and including $(R/|a|)^2$ effects is straightforward and does not require any additional three-body input [30, 31]. (For a general analysis of the order in $R/|a|$ at which three-body input is first needed in a given nd partial wave, see Ref. [32].)

These efforts open the way for precision calculations of three-body observables in EFT($\not\pi$). Calculations of three-body observables in this EFT are much simpler than in the χEFT, and the computational effort is significantly smaller. This is particularly so near the critical trajectory, where the χEFT is trying to bridge a huge range of distance scales: from a short-distance scale $1/\Lambda_\chi$ of fractions of a fermi to an NN scattering length of literally hundreds of fermis. The pionless EFT provides a natural way to build in the physics that occurs between the distance scale R and the unnaturally large scattering lengths that occur in this regime.

Therefore the χEFT and EFT($\not\pi$) offer mutually complementary approaches to an understanding of the quark-mass dependence of few-nucleon system observables. In order to use EFT($\not\pi$) to understand quark-mass dependence we, of course, need input from the χEFT, but once that input is in hand predictions for a variety of few-nucleon-system observables can be derived up to a given order in the $R/|a|$ expansion.

A first exploratory study along these lines was carried out in in EFT($\not\pi$) in Ref. [15]. The quark-mass dependence of the nucleon-nucleon scattering lengths from Ref. [14] was used as input to that calculation. In Ref. [33], a detailed investigation of the possibility that $1/a$ could vanish in both the $^3\mathrm{S}_1$ and $^1\mathrm{S}_0$ channels, *at the same* m_π was performed using an NN potential computed up to next-to-leading order (NLO) in the chiral expansion. The "critical" pion mass studied most thoroughly in Ref. [33] was $m_\pi^{crit} = 197.8577$ MeV. For that case the NLO χEFT calculation was matched to a leading-order (LO) EFT($\not\pi$) computation. The m_π-dependence of $1/a$ in both channels, as well as the pion-mass dependence of the triton binding energy, was used as input to that computation, and the spectrum of excited three-body states for m_π close to m_π^{crit} was computed. At LO that spectrum consists of an infinite tower of states with binding energies that obey:

$$\frac{B_3^{(n)}}{B_3^{(n+1)}} \approx 515.035, \tag{1}$$

where $B_3^{(n)}$ is the binding energy of the nth excited state in the tower. This LO prediction will be modified by higher-order terms in EFT($\not\pi$) which are larger for the more deeply bound states. Examining the 'data' of Ref. [33] for this ratio we see that it is 543 for $n = 0$ and 5.2×10^2 for $n = 1$. Here we show that EFT($\not\pi$) computations of the ratio $B_3^{(n)}/B_3^{(n+1)}$ converge rapidly for all $n \neq 0$, with the prediction (1) receiving corrections of at most 0.1% at NLO, and vanishingly small corrections at orders beyond that.

This extends the work of Ref. [33], because we use the same NLO χEFT calculation as input, but compute observables up to next-to-next-to-leading order (N^{2}LO) in EFT($\not\pi$). The work of Refs. [30, 31] shows that in order to do this the only additional information we need is the effective range in the $^3\mathrm{S}_1$ and $^1\mathrm{S}_0$ channels as a function of m_π. With these two effective ranges, together with knowledge of $1/a_s(m_\pi)$ and $B_d(m_\pi)$ and $B_3(m_\pi)$, we can use EFT($\not\pi$) to predict the behavior of the excited states of the three-body system and the doublet nd scattering length $a_{nd}^{1/2}$ as functions of m_π in a domain of m_π around m_π^{crit}. We also provide NLO predictions for the quartet nd scattering length $a_{nd}^{3/2}$ as a function of m_π.

In the process of providing these predictions we are presented with the opportunity to examine the convergence pattern of EFT($\not\pi$) in the three-nucleon sector. Since consideration of different pion masses yields different values of $R/|a|$, EFT($\not\pi$) will not converge at the same rate at all values of the pion mass. Furthermore, the presence of multiple three-nucleon bound states near the QCD critical trajectory provides us with the opportunity to examine how this EFT converges for bound states with different binding energies. In fact, we will find that near the critical trajectory the limiting factor in the accuracy of the calculations comes from corrections which scale as κR (with κ the momentum characteristic of the bound state being studied) and not from the often-quoted expansion parameter $R/|a|$, which is actually very small for m_π near m_π^{crit}.

This paper is structured as follows. In Section II we review the pertinent results obtained in chiral effective field theories for quark-mass dependence of observables in systems with $A = 0, 1, 2$, and 3. In Sec. III, we explain how these results are used as input to equations that describe neutron-deuteron scattering (and neutron-deuteron bound states) up to N^{2}LO in EFT($\not\pi$) . We present the results of our N^{2}LO computation in Sec. IV, together with a discussion of their convergence pattern and conclude in Sec. V.

II. CHIRAL EFFECTIVE FIELD THEORY

In order to understand the quark-mass dependence of hadronic observables we need a theory that encodes the soft breaking of QCD's $SU(2)_L \times SU(2)_R$ chiral symmetry by the quark mass term in the QCD Lagrangian. Chiral effective field theory is a low-energy theory with the same (low-energy) symmetries and pattern of symmetry breaking as QCD. As such it provides a systematic way to compute the quark-mass dependence of observables in few-nucleon systems.

In the $A = 0$ and $A = 1$ sectors the technology to do this is well-established, coming under the name "chiral perturbation theory" [2]. Scattering amplitudes are expanded in powers of the small parameter:

$$P \equiv \frac{m_\pi, p}{4\pi f_\pi, m_\rho} \tag{2}$$

where p is the typical momentum of the process under consideration. Since, according to the Gell-Mann-Oakes-Renner relation, $m_\pi^2 \sim m_q$, chiral perturbation theory provides access to quark-mass dependence, up to an accuracy that is determined by the order to which the computation is carried out.

In the $A = 0$ sector many observables have now been computed up to two loops, which is equivalent to a computation up to effects of $O(m_\pi^6) \equiv O(m_q^3)$. In the case of $A = 1$ most computations have been performed up to "complete one-loop order", which means that they include all effects up to $O(m_\pi^4) \equiv O(m_q^2)$.

For $A \geq 2$ the presence of non-perturbative effects makes the chiral counting more interesting. Weinberg proposed that the chiral perturbation theory expansion could be applied to the nucleon-nucleon potential in the $A = 2$ system, and, more generally, to the overall nuclear potential in a many-body system [3]. In this counting three-nucleon forces do not occur until next-to-next-to-leading order in the chiral expansion, and are suppressed by three powers of the small parameter [34]. The calculations of Refs. [15, 33] were based on a nuclear force computed up to $O(m_\pi^2) \equiv O(m_q)$ in the chiral expansion [35].

In this section, we review the relevant results on the quark-mass dependence of hadronic observables that entered that calculation. Since the results given there for the NN and NNN systems are only valid up to effects of $O(m_q)$ we in general do not provide expressions that go beyond this accuracy. We will see that present uncertainties in the quark-mass dependence of observables in the $A = 2$ system preclude reliable predictions for the m_q-dependence of three-body binding energies and scattering lengths. However, as long as there is a domain of m_q values where both NN scattering lengths become large with respect to $1/m_\pi$ then the approach of the Section III, that uses EFT($\not\pi$), together with a small amount of input from χEFT, to predict the quark-mass dependence of a variety of $A = 3$ observables, will always be applicable. This is true irrespective of the precise value of m_π^{crit}—or even whether the critical trajectory is only approximately realized. Therefore, EFT($\not\pi$) can always be used to propagate information from the χEFT through to few-nucleon system observables—as long as $|a| m_\pi \gg 1$ and $p/m_\pi \ll 1$. And, as the accuracy of the χEFT input to EFT($\not\pi$) improves, the results obtained using the expansion around the universal limit $|a| = \infty$ will become a better approximation to the quark-mass dependence of full QCD.

a. $A = 0$ At the order we work to here, quark-mass dependence is synonymous with pion-mass dependence because of the Gell-Mann-Oakes-Renner relation:

$$m_\pi^2 = -(m_u + m_d)\langle 0|\bar{u}u|0\rangle / f_\pi^2\,, \tag{3}$$

where $\langle 0|\bar{u}u|0\rangle \approx (-225 \text{ MeV})^3$ is the quark condensate, and $f_\pi = 92.4$ MeV is the pion-decay constant. In the following, we will therefore discuss all our results in terms of pion-mass dependence. This is more convenient for nuclear applications, since the pion mass is easy to adjust. The corresponding change in quark masses can then be read off from Eq. (3).

b. $A = 1$ The nucleon mass' dependence on m_π has now been calculated to complete two-loop order [36]. However, here we need only the result up to $O(m_q)$. This can be written as:

$$M = M_0 - 4c_1 m_\pi^2 + O(m_\pi^3), \tag{4}$$

where the leading non-analytic piece at $O(m_\pi^3)$ is easily calculated from the one-loop nucleon self-energy (in dimensional regularization with minimal subtraction), and the LEC c_1 is related to the nucleon σ-term. Meanwhile, M_0 is the nucleon mass in the chiral limit. If we take $c_1 = -0.81 \text{ GeV}^{-1}$ [37], we have $M_0 = 880$ MeV. Correspondingly, $M(m_\pi)$ increases to over a GeV at the putative critical pion mass $m_\pi \simeq 200$ MeV. Epelbaum *et al.* claim that this has only a small effect on spectra and so do not consider the effect of this change of M [14, 33]. Below we will provide an independent assessment of how this change in M affects the results near $m_\pi = m_\pi^{crit}$.

The other $A = 1$ quantity of relevance for our study of nuclear bound states is the pion-nucleon-nucleon coupling. For this we have the result:

$$\frac{g_{\pi NN}}{M} = \frac{g_A}{f_\pi}\left(1 + 2\Delta - \frac{2m_\pi^2}{g_A}\bar{d}_{18}\right), \tag{5}$$

where $g_A = 1.26$ is the physical value of the nucleon's axial coupling. This is the Goldberger-Treiman relation in the chiral limit, and here it is supplemented by an $O(m_q)$ term involving the LEC $\bar{d}_{18}$. Using a value of $g_{\pi NN}$ extracted from a phase-shift analysis of low-energy πN data [38, 39] we get $\bar{d}_{18} = -0.97 \text{ GeV}^{-2}$ [14]. Also appearing in Eq. (5) is the ratio Δ, which encodes the m_q-dependence of the ratio g_A/f_π. Δ is just the fractional change in this ratio at an arbitrary value of m_π, as compared to the value at the physical m_π, m_π^{phys}, i.e.:

$$\Delta \equiv \frac{(g_A/f_\pi)_{m_\pi} - (g_A/f_\pi)_{m_\pi^{phys}}}{(g_A/f_\pi)_{m_\pi^{phys}}} \tag{6}$$

The expression for Δ in terms of low-energy constants appearing in $\mathcal{L}_{\pi N}^{(3)}$ and $\mathcal{L}_{\pi\pi}^{(4)}$ can be found in Ref. [33].

c. $A = 2$ The quark-mass dependence of the chiral NN interaction was calculated to next-to-leading order (NLO) in the chiral counting in Refs. [12, 13, 14]. In addition to the quark-mass dependence of the pion mass and πNN coupling that appear in the one-pion-exchange potential the short-distance part of the force acquires a quark-mass dependence of its own. This is essential for correct renormalization [40]. This quark-mass dependence can be described by parameters D_s and D_t, so that the NN potential in a particular S-wave (t=^{3}S$_1$, s=^{1}S$_0$) is:

$$V = C_{s/t} + D_{s/t}\left[m_\pi^2 - (m_\pi^{phys})^2\right] + V_{OPE} + V_{TPE}^{(2)}, \tag{7}$$

where V_{OPE} is the (partial-wave projected) one-pion exchange with the already discussed variation in $g_{\pi NN}$ (5) and m_π (3) taken into account, and $V_{TPE}^{(2)}$ is the well-known "leading" two-pion exchange [35, 41, 42]. Note that to the order considered here it is only necessary to take into account the m_π-dependence of $g_{\pi NN}$ (or, equivalently, g_A and f_π) in the LO piece

of the NN potential. We do not take into account the m_π-dependence of g_A and f_π in the two-pion-exchange potential but instead simply use their physical values there. Considering only "explicit" m_π dependence in $V_{TPE}^{(2)}$ is sufficient at the order we work to here.

Meanwhile, in Ref. [33] the unknown parameters $D_{s/t}$ were converted into dimensionless numbers via:

$$\alpha_{s/t} \equiv \frac{f_\pi^2 \Lambda_\chi^2 D_{s/t}}{16\pi} \tag{8}$$

At present next-to-nothing is known about the values of α. But predictions for the pion-mass dependence of S-wave scattering can be obtained by varying the α's within naturalness bounds. The uncertainty in the behavior of Δ as a function of m_π then further enlarges the range of results obtained for, say, the NN scattering lengths as a function of m_π.

Because of these uncertainties, the study of Ref. [33] did not attempt to predict the precise value of the critical pion mass where the inverse scattering lengths in both S-waves vanish. This strategy is motivated not just by ignorance as regards the two LECs appearing in the α's, but also because we have not considered the impact that $m_u \neq m_d$ would have on the NN potential. Such effects must be included if the Braaten-Hammer conjecture, as originally formulated, is to be investigated [15]. Instead, in Ref. [33] α parameters were chosen in such a way that a critical trajectory occurred. For critical pion masses in the range 175 MeV $\leq m_\pi^{crit} \leq$ 205 MeV, it is always possible to find an appropriate set of α parameters. Three sets of α parameters were given in Ref. [33], with each one corresponding to a different critical pion mass m_π^{crit}. The computations of Ref. [33] focused particularly on a choice $\alpha_t = -2.5$, which yields $\alpha_s = 2.138598$ and a critical pion mass $m_\pi^{crit} = 197.8577$ MeV. Although it is unlikely that physical QCD will correspond to this particular solution, many aspects of the limit cycle are universal and do not depend on the exact parameter values [21]. Therefore in what follows we take the results reported in Ref. [33] for this choice of χEFT parameters as both the input data for EFT($\not\pi$) and the experimental data to which we will compare our EFT($\not\pi$) results for the pion-mass dependence of three-nucleon observables in the vicinity of the QCD critical trajectory.

As already discussed in the introduction, the NN inputs we need from the χEFT for our NNLO EFT($\not\pi$) calculation are scattering lengths and effective ranges in the spin-triplet and spin-singlet channels. The scattering lengths a_t and a_s can, of course, be exchanged for the momenta γ_t and γ_s characterizing the position of the bound-state/virtual-state poles in the two-body propagator. If higher-order terms in the effective-range expansion are neglected, the relation between the two quantities is simply

$$\gamma_\alpha = \frac{1}{r_\alpha}\left(1 - \sqrt{1 - 2r_\alpha/a_\alpha}\right) , \tag{9}$$

with $\alpha = s, t$ indicating a particular NN channel. The advantage of using γ_α, rather than a_α, is that the NN pole position is not modified by higher-order corrections. In the following, we will therefore use $\gamma_t(m_\pi)$, $\gamma_s(m_\pi)$, $r_t(m_\pi)$, and $r_s(m_\pi)$ as the NN input.

The behavior of the input pole momenta $\gamma_s(m_\pi)$ and $\gamma_t(m_\pi)$ in the vicinity of $m_\pi = m_\pi^{crit}$ is depicted in the inset in the left panel of Fig. 1. As promised, the pole momenta vanish at the critical value of the pion mass $m_\pi^{crit} = 197.8577$ MeV. For pion masses below m_π^{crit} $\gamma_t(m_\pi) > 0$ and the deuteron is bound. As $\gamma_t(m_\pi)$ decreases, the deuteron becomes more and more shallow and finally becomes unbound at the critical pion mass. Above the critical pion mass the deuteron exists as a shallow virtual state. In the spin-singlet channel, the situation is reversed: the "spin-singlet deuteron" is a virtual state below the critical pion mass and

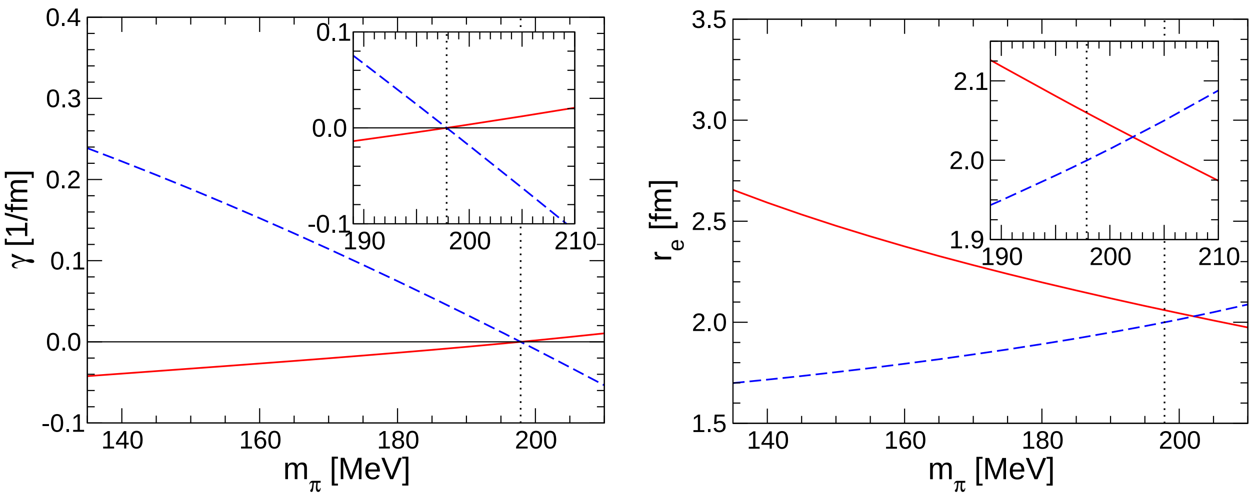

FIG. 1: Left panel: Pole momenta in the $^3S_1$ (dashed line) and $^1S_0$ (solid line) nucleon-nucleon channels as a function of the pion mass m_π (from Ref. [33]). The vertical dotted line indicates the critical pion mass m_π^{crit} while the inset shows the critical region in more detail. Right panel: same for the effective ranges (from Ref. [43]).

becomes bound above. In the right panel of Fig. 1 we show the corresponding dependence of the spin-singlet and spin-triplet effective ranges [43]. The pion-mass dependence of the effective ranges is weak and both are close to 2 fm throughout the region displayed. In the region of interest $r_s(m_\pi)$ decreases monotonically as the pion mass is increased whereas $r_t(m_\pi)$ increases. At a pion mass of about 202 MeV the curves cross.

Above we pointed out that the results of Refs. [33, 43] which are presented in Fig. 1 do not include effects due to the pion-mass dependence of the nucleon mass. Such effects can easily be accounted for though, by noting that the computations presented in Fig. 1 are done in a non-relativistic framework, and no $1/M$ corrections to the NN potential are incorporated. Consequently the nucleon mass can be scaled out of the problem by an appropriate choice of units. The critical pion mass is then written as:

$$m_\pi^{crit} = 0.2107M, \tag{10}$$

where we have employed an (isospin-averaged) nucleon mass of $M = 938.9$ MeV. A value of m_π^{crit} in MeV that includes the impact of $M(m_\pi)$ can be obtained from Eq. (10) by inserting the expression (4) for $M(m_\pi^{crit})$ in place of M on the right-hand side, and solving the resulting equation for m_π^{crit}. This yields $m_\pi^{crit} = 220$ MeV, with the accuracy limited to two digits by the precision with which c_1 is known.

We can use the same argument to assess the impact of the m_π-dependence of M on two-body observables when $m_\pi \neq m_\pi^{crit}$. Incorporating the pion-mass dependence of the nucleon mass in the calculation of Refs. [33, 43] in this way would thus lead to a change of the scale on both axes in the left panel of Fig. 1 by a factor of $M(m_\pi)/M$. The x-axis in the right panel would be rescaled by the same factor, while the y-axis there would be rescaled by $M/M(m_\pi)$. The effect of such rescaling is largest at the highest pion masses considered, but even there it is less than 15%. Other uncertainties in the calculation of the functions $\gamma_s(m_\pi)$, $\gamma_t(m_\pi)$, $r_s(m_\pi)$, and $r_t(m_\pi)$ are larger than this, and so from here on we follow the procedure of Refs. [33, 43] and ignore effects on these quantities due to the pion-mass dependence of M.

d. A=3 We also need one three-body datum as input to EFT($\not\pi$) in order to perform our N^{2}LO computation of three-body system observables. In Ref. [33], the binding energies of the triton and the first two excited states in the vicinity of the limit cycle were obtained from the solution of the Faddeev equations for the NLO χEFT potential. For much of the pion-mass range of interest to us there is only one bound state, and so, in that region, $100 \leq m_\pi \leq 190$ MeV, we renormalize EFT($\not\pi$) using the binding energy of the triton ground state, $B_3^{(0)}$, and then predict the nd doublet scattering length, $a_{nd}^{1/2}$. But our results for pion-mass dependence are particularly interesting in the "critical region", which we define to be values of m_π for which the triton has at least one excited state. For the choice $m_\pi^{crit} = 197.8577$ MeV the calculations of Ref. [33] indicate a critical region corresponding to 190 MeV $\leq m_\pi \leq$ 210 MeV. The first excited state that is present in this region is much shallower than the ground state, and is transparently within the domain of validity of EFT($\not\pi$) . Thus errors in that EFT are smaller if we renormalize to its binding energy, $B_3^{(1)}$, rather than to $B_3^{(0)}$. The EFT($\not\pi$) result for $B_3^{(0)}$ then becomes a prediction and we can also predict $a_{nd}^{1/2}$. The χEFT results for both the ground and first-excited state in the "critical region" are shown in Fig. 2, together with our N^{2}LO EFT($\not\pi$) calculation.

III. THE PIONLESS EFT TO N^{2}LO

In the critical region where there is more than one three-nucleon bound state, the length scales in the three-nucleon problem change rapidly as m_π is varied. The binding energy of the deepest lying three-nucleon state changes slowly, and is still within a factor of two of its experimental value when m_π^{crit} is reached. However, in this region the neutron-deuteron scattering length varies between $-\infty$ and ∞, and does so an infinite number of times. A single cycle between -∞ and ∞ takes place over the range of pion-mass increase that is needed to make an additional shallow three-nucleon ("Efimov") state appear as $m_\pi \to m_\pi^{crit}$. Consequently, the numerical effort which has to be devoted to the calculation of three-nucleon observables increases significantly once m_π is large enough that the first Efimov state appears—or is close to appearing. We advocate determining the dependence of key two- and three-nucleon observables on the pion mass with χEFT, then using those results as input to the simpler EFT($\not\pi$) and employing that EFT to analyze the behavior of other three-nucleon observables in the critical region.

EFT($\not\pi$) is a systematic expansion in contact interactions where—for momenta $k \sim 1/a$—the small expansion parameter is R/a. The corresponding low-energy Lagrangian for the neutron-deuteron system is given by [26]

$$\begin{aligned}\mathcal{L} \;=\;& N^\dagger(i\partial_0 + \frac{\nabla^2}{2M})N - t_i^\dagger(i\partial_0 + \frac{\nabla^2}{4M} - \Delta_t)t_i - s_j^\dagger(i\partial_0 + \frac{\nabla^2}{4M} - \Delta_s)s_j \\ &+ g_t\left(t_i^\dagger N^T\tau_2\sigma_i\sigma_2 N + \text{h.c}\right) + g_s\left(s_j^\dagger N^T\sigma_2\sigma_j\tau_2 N + \text{h.c}\right) \\ &- G_3 N^\dagger\left(g_t^2(t_i\sigma_i)^\dagger t_{i'}\sigma_{i'} + \frac{1}{3}g_t g_s[(t_i\sigma_i)^\dagger s_j\tau_j + \text{h.c}] + g_s^2(s_j\tau_j)^\dagger s_{j'}\tau_{j'}\right)N + \ldots\ , \end{aligned} \tag{11}$$

where N represents the nucleon field and $t_i(s_j)$ are the di-nucleon fields for the $^3\mathrm{S}_1$ ($^1\mathrm{S}_0$) channels with the corresponding quantum numbers, respectively. The σ_i (τ_j) are Pauli matrices in spin (isospin) space, respectively, and the dots indicate additional terms with more fields/derivatives.

To renormalize three-nucleon observables in the nd $\mathrm{S}_{1/2}$ channel within this framework, a three-nucleon force symmetric under $SU(4)$ spin-isospin rotations [26] (here denoted by G_3) or *equivalently* a subtraction has to be performed [44, 45]. Therefore, one three-body input parameter is needed for the calculation of observables in this channel—the one in which the triton exists.

In order to compute three-nucleon observables we need the full two-body propagator τ, which is the result of dressing the bare di-nucleon propagator by nucleon loops to all orders. The EFT is arranged to reproduce the effective-range expansion for τ, i.e.

$$\tau_\alpha(E) = -\frac{2}{\pi M} \frac{1}{-\gamma_\alpha + \sqrt{-ME} + \frac{r_\alpha}{2}\left(\gamma_\alpha^2 + ME\right)} \ , \tag{12}$$

where E denotes the two-body energy in the two-body c.m. frame, γ_α gives the NN pole position, r_α is the effective range, and the index $\alpha = s, t$ indicates either the singlet or triplet NN channel. In the triplet channel the pole position γ_t is related to the deuteron binding energy $B_d = \gamma_t^2/M$. The form (12) cannot be directly used as input to EFT three-nucleon calculations because it has poles at energies outside the domain of validity of the EFT. Therefore, the propagator cannot be employed within a three-body integral equation which has cutoffs $\Lambda > 1/r_\alpha$ unless additional techniques to subtract these unphysical poles are implemented. Instead of using the propagator in the form above we will expand it to nth order in R/a:

$$\tau_\alpha^{(n)}(E) = \frac{S_\alpha^{(n)}(E)}{E + \gamma_\alpha^2/M}. \tag{13}$$

For $n < 3$, the residue $S^{(n)}$ is given by

$$S_\alpha^{(n)}(E) = \frac{2}{\pi M^2} \sum_{i=0}^{n} \left(\frac{r_\alpha}{2}\right)^i [\gamma_\alpha + \sqrt{-ME}]^{i+1} \ , \tag{14}$$

while for $n \geq 3$ higher-order terms in the effective-range expansion contribute to $S(E)$. The set of integral equations for the nucleon-deuteron K-matrix generated by this EFT (neglecting, for the moment, the nd coupling G_3) is given by [26, 45]

$$\begin{aligned}
K_{tt}^{(n)}(q,q';E) \ &= \ \mathcal{Z}_{tt}(q,q';E) + \mathcal{P}\int_0^\Lambda \mathrm{d}q''\, q''^2 \mathcal{Z}_{tt}(q,q'';E)\tau_t^{(n)}(E - \frac{3}{4}\frac{q''^2}{M})K_{tt}^{(n)}(q'',q';E) \\
&\quad + \mathcal{P}\int_0^\Lambda \mathrm{d}q''\, q''^2 \mathcal{Z}_{ts}(q,q'';E)\tau_s^{(n)}(E - \frac{3}{4}\frac{q''^2}{M})K_{st}^{(n)}(q'',q';E) \ , \\
K_{st}^{(n)}(q,q';E) \ &= \ \mathcal{Z}_{st}(q,q';E) + \mathcal{P}\int_0^\Lambda \mathrm{d}q''\, q''^2 \mathcal{Z}_{st}(q,q'';E)\tau_t^{(n)}(E - \frac{3}{4}\frac{q''^2}{M})K_{tt}^{(n)}(q'',q';E) \\
&\quad + \mathcal{P}\int_0^\Lambda \mathrm{d}q''\, q''^2 \mathcal{Z}_{ss}(q,q'';E)\tau_s^{(n)}(E - \frac{3}{4}\frac{q''^2}{M})K_{st}^{(n)}(q'',q';E) \ ,
\end{aligned} \tag{15}$$

where n is the order of the calculation (in what follows we assume $n < 3$) and $\mathcal{P}$ indicates a principal-value integral. The formulation in terms of the K-matrix is useful as long as we

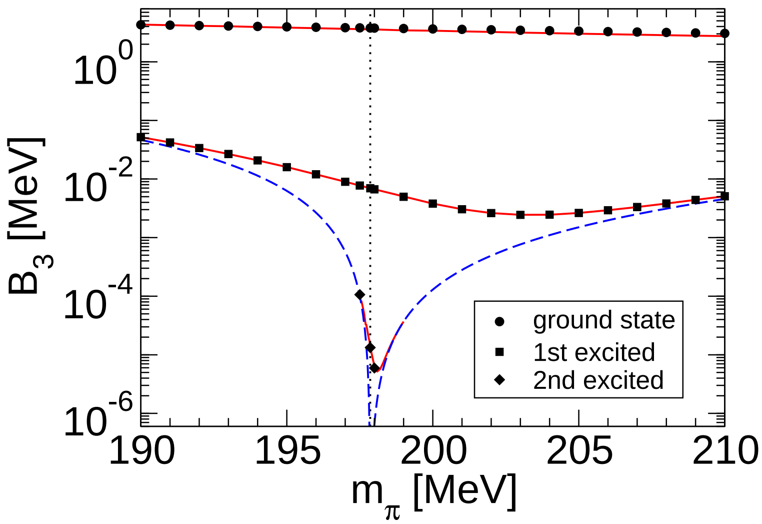

FIG. 2: Triton ground and excited state energies B_3 in the critical region. The circles (ground state), squares (first excited state), and diamonds (second excited state) give the χEFT result, while the solid lines are calculations in the pionless theory to N^{2}LO. The vertical dotted line indicates the critical pion mass m_π^{crit}. The thresholds for three-nucleon states to be stable against breakup into a single nucleon plus an NN bound state are given by the dashed lines. The zero of energy corresponds to the opening of the 3N channel.

are only interested in bound states or nd scattering below the three-nucleon threshold. The Born amplitude $\mathcal{Z}_{\alpha\beta}$ is given by

$$\mathcal{Z}_{\alpha\beta}(q,q';E) = -\lambda_{\alpha\beta}\frac{M}{qq'}\log\left(\frac{q^2+qq'+q'^2-ME}{q^2-qq'+q'^2-ME}\right) , \tag{16}$$

with the isospin matrix

$$\lambda_{\alpha=\{s,t\};\,\beta=\{s,t\}} = \frac{1}{4}\begin{pmatrix} 1 & -3 \\ -3 & 1 \end{pmatrix} . \tag{17}$$

Below three-nucleon breakup threshold the K-matrix is related to nd phaseshifts through

$$K(k,k;E) \;=\; -\frac{3M}{8\gamma_t k}\tan\delta \, . \tag{18}$$

In Refs. [30, 31], it was shown that the use of one subtraction allows $\tau^{(n)}$ up to N^{2}LO ($n=2$) to be inserted in Eqs. (15) with cutoff-independent predictions resulting. This is in marked contrast to the unsubtracted equations written above, which generate cutoff variation of $O(1)$ in low-energy observables if left unrenormalized [26, 46]. The price that is paid for the improved ultraviolet behavior of the subtracted equations is that $a_{nd}^{1/2}$ appears as an input parameter in the integral equation. For further details on this subtraction method, we refer to Refs. [30, 45]. In the next section we will use the subtracted equations to perform calculations in the pionless EFT up to N^{2}LO.

To close this section we note that the Lagrangian (11) is symmetric under Wigner $SU(4)$ spin-isospin rotations provided $g_s = g_t$ and $\Delta_s = \Delta_t$. Moreover, the integral equations (15) have an approximate $SU(4)$ symmetry for momenta $q \gg \gamma_s, \gamma_t$, even if $g_s \neq g_t$ or

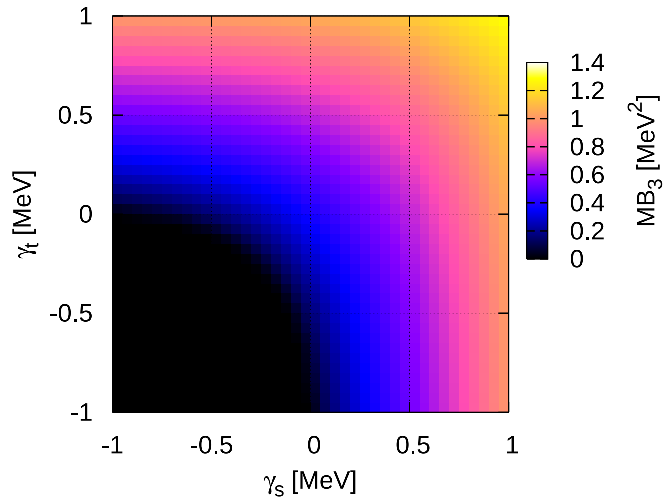

FIG. 3: Binding energy B_3 of an excited state of the triton as a function of γ_s and γ_t in the vicinity of m_π^{crit}. The computation is performed here to leading order in EFT($\not\pi$) .

$\Delta_s \neq \Delta_t$. (For a discussion of this symmetry for the NN system see Ref. [47].) Because of this symmetry, an $SU(4)$-symmetric three-body force is sufficient for renormalization [26]. In Fig. 3, we illustrate a manifestation of this symmetry in the bound-state spectrum calculated at LO in EFT($\not\pi$). We show the binding energy of a triton excited state in the critical region as a function of γ_s and γ_t. In the lower left corner, the considered triton state does not exist. As γ_s and γ_t approach zero, the state appears at threshold and then becomes more and more bound. The figure is clearly symmetric under reflection on the main diagonal corresponding to a specific spin-isospin rotation that exchanges γ_s and γ_t.

Beyond leading order in EFT($\not\pi$) $SU(4)$-breaking effects enter the computation through the difference in singlet and triplet effective ranges $r_s - r_t$. The right-hand panel of Fig. 1 displays the interesting feature that—at least for the choice of χEFT short-distance coefficients being studied here—$r_s - r_t$ vanishes at a pion mass only a little larger than m_π^{crit}. As remarked upon in Ref. [33], this results in $SU(4)$-breaking effects near the critical point that are much smaller than one might naively expect, since $r_s - r_t \ll R$, the range of the NN interaction. More generally, Fig. 1 suggests that a suitable choice of α_s and α_t could lead to $r_s - r_t = \gamma_s = \gamma_t = 0$ at a single "$SU(4)$ critical pion mass". It is unclear whether a χEFT that has this feature has anything to do with QCD. But the EFT($\not\pi$) valid near a critical trajectory which also has $r_s = r_t$ could be built using $SU(4)$-symmetric operators for the R/a expansion, with $SU(4)$ breaking additionally suppressed by another small parameter.

IV. RESULTS

In this section, we solve the once-subtracted version of the integral equations (15) for pion masses in the range 100 MeV $\leq m_\pi \leq$ 200 MeV. Two-nucleon pole positions and effective ranges for the relevant χEFT solution were displayed in Fig.1, and in the critical region we

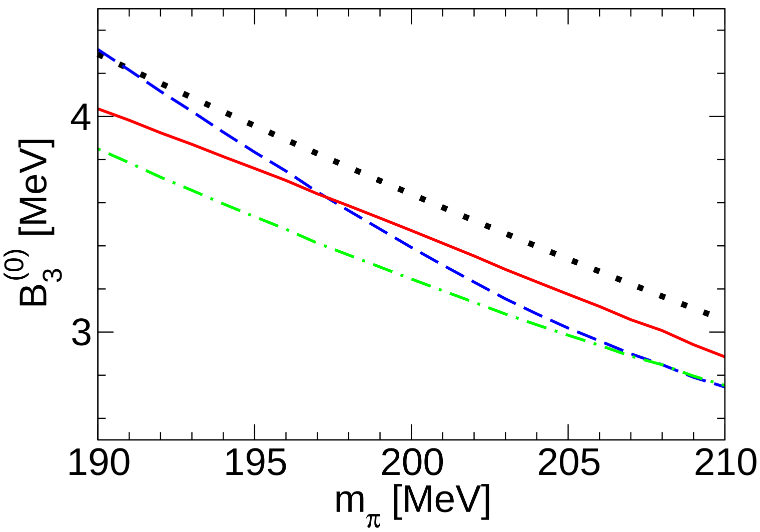

FIG. 4: Binding energy of the triton ground state in the critical region computed in the pionless EFT at LO (dashed), NLO (dash-dotted) and N^{2}LO (solid). The dotted line gives the (interpolated) χEFT results for comparison.

take as our one three-body input the energy of the first triton excited state $B_3^{(1)}$. We provide a detailed discussion of the critical region, and also examine the behavior of EFT($\not\pi$) for pion masses between the critical region and the physical value. In the latter case the three-body datum chosen as input is the triton binding energy $B_3^{(0)}$.

A. Bound-State Spectrum

Turning first to the critical region, we display the results obtained from solving the homogeneous version of Eq. (15) for negative energies. The spectrum of triton states as a function of m_π at N^{2}LO is shown in Fig. 2, and compared to the χEFT result.

The binding energies from χEFT are given in Fig. 2 by the circles ($B_3^{(0)}$), squares ($B_3^{(1)}$), and diamonds ($B_3^{(2)}$) [33]. The dashed lines indicate the neutron-deuteron ($m_\pi \leq m_\pi^{crit}$) and neutron-spin-singlet-deuteron ($m_\pi \geq m_\pi^{crit}$) thresholds. For B_3 less than these energies three-body states are unstable against breakup into the $1+2$ configuration. Directly at the critical pion mass, these thresholds coincide with the three-body threshold and the triton has infinitely many excited states. The solid lines show our N^{2}LO calculation in the pionless EFT where the first triton excited state was used as input. Our results for the second excited state and the ground state reproduce the χEFT results very well. An important point here is that the binding energy of the triton ground state varies only weakly over the whole range of pion masses. Indeed $B_3^{(0)}(m_\pi^{crit}) \approx 0.5 B_3^{(0)}(m_\pi^{phys})$. The excited states are influenced by the $1+2$ threshold and their energies vary more strongly.

In order to study the convergence of the EFT($\not\pi$) more thoroughly we now look at the prediction for the triton ground-state energy in some detail. In Fig. 4, we show our results for the binding energy of the three-nucleon ground state for pion masses in the "critical region" The dashed, dash-dotted, and solid lines denote, respectively, the LO, NLO, and N^{2}LO results for the triton ground-state energy, while the dotted line gives the (interpolated)

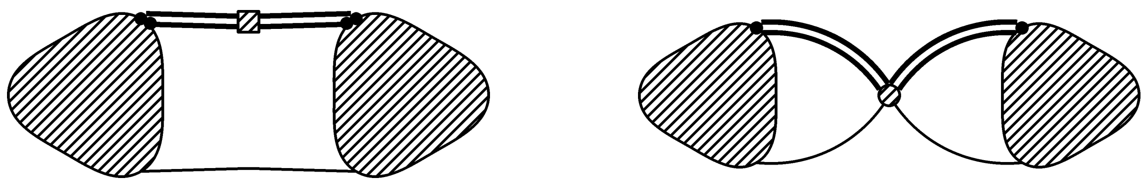

(1) (2)

FIG. 5: Diagrams contributing to the NLO shift in the binding energies. The shaded square in Diagram 1 represents a non-trivial effective-range insertion. The shaded circle in Diagram 2 denotes the insertion of the subleading three-body force H_1. The shaded blobs are LO nd vertex functions.

χEFT result of Ref. [33]. The leading-order EFT($\not\pi$) results describe χEFT's $B_3^{(0)}(m_\pi)$ curve surprisingly well, although the shape of the m_π-dependence is clearly wrong. The NLO computation does not seem to yield significant improvement in the overall agreement. The results of our N^{2}LO calculation are on average better than the LO results.

At first sight this slow convergence is surprising, since the parameter $\gamma r \to 0$ at $m_\pi = m_\pi^{crit}$. But this simply means that the slow convergence in the critical region must be due to the significant (compared to $1/r$) binding momentum $\kappa = \sqrt{4MB_3/3}$, which is about 65 MeV in this pion-mass range.

B. Understanding Range Corrections in EFT($\not\pi$)

A rough estimate of the impact of higher-order corrections on EFT($\not\pi$) predictions can be obtained by applying naive dimensional analysis. The relevant scales for the orders under consideration are γ, r and the binding momentum κ. (For simplicity we will drop the indices s and t in the ensuing discussion since the scaling with r_s and r_t is the same.) It follows therefore that the error for an arbitrary three-body observable O_3 at order j should scale as

$$\frac{\Delta O_3}{O_3} \approx A_{j+1}\left(\frac{kr}{2}\right)^{j+1} + B_{j+1}(\gamma r)^{j+1}\,, \tag{19}$$

where A_{j+1} and B_{j+1} are (observable-dependent) numbers of order one, and k is the momentum associated with O_3.

However, this naive estimate clearly fails to explain the pattern of convergence displayed in Fig. 2. A more thorough understanding of this pattern of corrections can be gained by examining the way that the NLO correction at the critical pion mass scales with the parameters κ and r. We will analyze a perturbative expansion of EFT($\not\pi$) about the LO result [28]. When $m_\pi = m_\pi^{crit}$, $\gamma = 0$ and γr corrections do not exist. In this "scaling limit", the two-body propagator at NLO simplifies to

$$\tau^{(1)}(E) = -\frac{2}{\pi M}\left[\frac{1}{\sqrt{-ME}} + \frac{1}{\sqrt{-ME}}\left(-\frac{r}{2}ME\right)\frac{1}{\sqrt{-ME}}\right]\,. \tag{20}$$

In Fig. 5 we display the diagrams which have to be taken into account for analysis of κr corrections. Diagram (1) represents a perturbative insertion of $r/2$, à la the second term

of Eq. (20). Diagram (2) denotes the inclusion of the subleading three-body force H_1. The presence of H_1 is necessary in order to absorb a divergence produced by diagram (1), but H_1 always appears in a fixed combination with H_0, i.e. it does not need to be determined by any additional three-body data [28].

An analysis of the superficial degree of divergence of these diagrams gives amplitudes which scale with momentum p as:

$$\mathcal{M}^{(1)} \sim -\frac{rp}{2M}; \quad \mathcal{M}^{(2)} \sim \frac{H_1 p^2}{M^2}. \tag{21}$$

However, the only remaining momentum scale in the problem is the binding momentum for the bound state under consideration, i.e. $\kappa^{(n)}$. The NLO shift in the binding energy of the nth bound state is therefore

$$\Delta B_3^{(n)} = Z\left(\alpha \frac{r}{2M}\kappa^{(n)} - \beta \frac{H_1}{M^2}\kappa^{(n)2}\right) , \tag{22}$$

where α and β are numbers of order one, which, due to the discrete scale invariance of the LO spectrum in EFT($\not\pi$) , are independent of n. Z denotes the wave-function renormalization, and a similar diagrammatic analysis leads us to conclude that $Z \sim \left(\kappa^{(n)}\right)^2$. We therefore obtain

$$\Delta B_3^{(n)} = \left(\tilde{\alpha}\frac{r}{2M}\left(\kappa^{(n)}\right)^3 - \tilde{\beta}\frac{H_1}{M^2}\left(\kappa^{(n)}\right)^4\right) . \tag{23}$$

If we have renormalized to the experimental binding energy of the mth bound state at leading order we want to preserve that experimental value at NLO, and so we demand $\Delta B_3^{(m)} = 0$. This fixes the strength of H_1 to be

$$H_1 = \frac{\tilde{\alpha} r M}{2\tilde{\beta}}\frac{1}{\kappa^{(m)}} , \tag{24}$$

and the shift in the binding energy of the nth state therefore becomes

$$\frac{\Delta B_3^{(n)}}{B_3^{(n)}} = \tilde{\alpha}\frac{\kappa^{(n)} r}{2}\left(1 - \frac{\kappa^{(n)}}{\kappa^{(m)}}\right) . \tag{25}$$

Parametrically, the fractional change in $B_3^{(n)}$ is of order $\kappa^{(n)} r$, as expected. However, the number in brackets in Eq. (25) is not necessarily of order 1, since the ratios of binding momenta are large. Because of the discrete scaling symmetry of the three-nucleon spectrum which is realized in our LO EFT($\not\pi$) calculation we have

$$\frac{\kappa^{(n)}}{\kappa^{(m)}} = (22.7)^{m-n}. \tag{26}$$

If the state which has been used as a renormalization point (m) is more weakly bound than the states for which we are making a prediction (n) we have $m > n$, and so the NLO shift will be amplified by a factor of $(22.7)^{m-n}$. This to some extent explains the rather large shift in $B_3^{(0)}$ when we renormalize to $B_3^{(1)}$. Conversely, if the state used for renormalization is more strongly bound then the state under consideration, and so $m < n$, the NLO shift will be

$$\frac{\Delta B_3^{(n)}}{B_3^{(n)}} \approx \tilde{\alpha}\frac{\kappa^{(n)} r}{2}, \tag{27}$$

	$B_3^{(0)}$ [MeV]	$B_3^{(0)}/B_3^{(1)}$	$B_3^{(2)}$ [MeV]	$B_3^{(1)}/B_3^{(2)}$
LO	3.579	515	$1.349 \cdot 10^{-5}$	515.0
NLO	3.369	485	$1.350 \cdot 10^{-5}$	514.8
N^{2}LO	3.594	517	$1.350 \cdot 10^{-5}$	514.8
χEFT	3.774	543	$1.329 \cdot 10^{-5}$	523.1

TABLE I: Binding energies $B_3^{(0)}$ and $B_3^{(2)}$ and ratios $B_3^{(0)}/B_3^{(1)}$ and $B_3^{(1)}/B_3^{(2)}$ at the critical pion mass. The three-body input parameter has been adjusted such that the χEFT result for the first excited triton state $B_3^{(1)} = 0.00695$ MeV (at $m_\pi = m_\pi^{crit}$) is reproduced. The first three rows show the results in the pionless EFT at LO, NLO, and N^{2}LO, while the last row gives the χEFT result from Ref. [33].

in accordance with naive dimensional analysis.

Equation (25) predicts that EFT($\not{\pi}$) should converge more smoothly for states which are less bound than the state which has been used for renormalization. So we now turn our attention to the convergence of predictions for binding energies of excited states of the triton, where we expect EFT($\not{\pi}$) to work much better than it does for the ground state. Since we used $B_3^{(1)}$ as input, the simplest observable we can test this hypothesis on is the ratio $B_3^{(1)}/B_3^{(2)}$. (Later we will examine the doublet nd scattering length, $a_{nd}^{1/2}$, but there we do not have χEFT data with which to compare.) Using Eq. (25), and remembering that we are effectively choosing H_1 such that $\Delta B_3^{(1)} = 0$, we expect

$$\frac{B_3^{(1)}}{B_3^{(2)}} \approx 515 \times \left(1 - \tilde{\alpha}\frac{\kappa^{(2)}r}{2} + \ldots\right) \ , \tag{28}$$

with $\kappa^{(2)}$ the binding momentum of the second excited state. Since $\kappa^{(2)}r/2 < 0.1\%$, this suggests that $B_3^{(1)}/B_3^{(2)}$ will change by less than 0.1% from LO to N^{2}LO.

In Table I we show the ratios of the first three Efimov states extracted from the χEFT and pionless EFT calculations. In Ref. [33] values of 542.9 and 523.1 were given for $B_3^{(0)}/B_3^{(1)}$ and $B_3^{(1)}/B_3^{(2)}$ respectively. Given Eq. (25) we expect that EFT($\not{\pi}$) converges slowly for binding momenta on the order of $\kappa^{(0)}$, so we do not anticipate reproduction of $B_3^{(0)}/B_3^{(1)}$ with accuracy better than a few per cent at N^{2}LO. This expectation is borne out by the results of Table I.

In contrast, range corrections are miniscule in the case of $B_3^{(1)}/B_3^{(2)}$. We have calculated NLO and N^{2}LO κr corrections to this ratio at $m_\pi = m_\pi^{crit}$. We find a shift at NLO in the ratio that is numerically significant, and on the order of the expected 0.1%. No N^{2}LO shift in $B_3^{(1)}/B_3^{(2)}$ is seen within our numerical accuracy. We summarize this result as:

$$\frac{B_3^{(1)}}{B_3^{(2)}} = 514.8 \pm 0.02 \pm 0.0004, \tag{29}$$

where the first error is from the numerical precision of our calculation, and the second is from higher-order terms in the EFT($\not{\pi}$) expansion. We note that the χEFT calculation of this

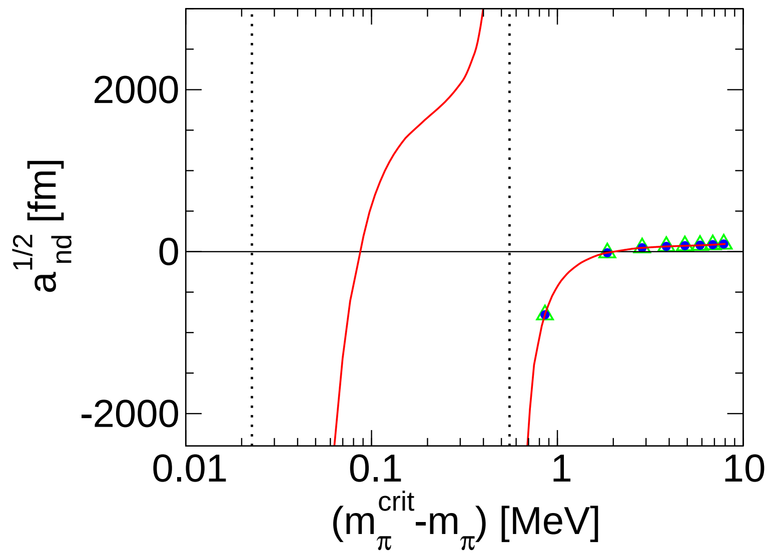

FIG. 6: Doublet neutron-deuteron scattering length $a_{nd}^{1/2}$ in the critical region computed in the pionless EFT. The solid line gives the LO result, while the triangles and circles show the NLO and N^{2}LO results. The dotted lines indicate the pion masses at which $a_{nd}^{1/2}$ diverges.

quantity is numerically quite delicate, since it requires a momentum mesh that bridges scales ranging from $\Lambda = 540$ MeV (the cutoff in the chiral potential) to the binding momentum $\kappa^{(2)} \approx 130$ keV—more than three orders-of-magnitude difference. Indeed, reexamination of the calculation of the second excited-state energy in Ref. [33] showed that the numerical value of 523.1 quoted there is only accurate to two significant digits [48]. There is thus no disagreement between our result (29) and that quoted in Ref. [33]. This emphasizes the ability of EFT($\not\pi$) to easily obtain high-precision results for three-body observables.

Therefore, at the critical pion mass, $B_3^{(1)}/B_3^{(2)}$ differs from the Efimov prediction (1) by less than 0.1%. This allows us to predict that the higher excited states will obey

$$\frac{B_3^{(1)}(m_\pi^{crit})}{B_3^{(n+1)}(m_\pi^{crit})} = (515)^n. \tag{30}$$

for all $n \geq 1$. This result, which is a rigorous consequence of the discrete scaling symmetry of the Efimov spectrum and the scaling of the corrections to that spectrum, could be a useful constraint on the infinite tower of excited states if the critical trajectory is ever realized in a lattice QCD computation.

C. Doublet Scattering Length

Scattering observables have not been calculated in χEFT in the vicinity of the critical trajectory, but can be predicted in EFT($\not\pi$) in a straightforward way. In principle the subtracted version of Eq. (15) can be solved at any positive energy to obtain nd phaseshifts. In practice additional numerical techniques are needed to do this above the three-nucleon breakup threshold, and at the critical pion mass this coincides with the nd threshold. However, the technology to deal with this complication is well known. Here we examine the nd scattering lengths as a representative of all nd scattering observables that could be computed

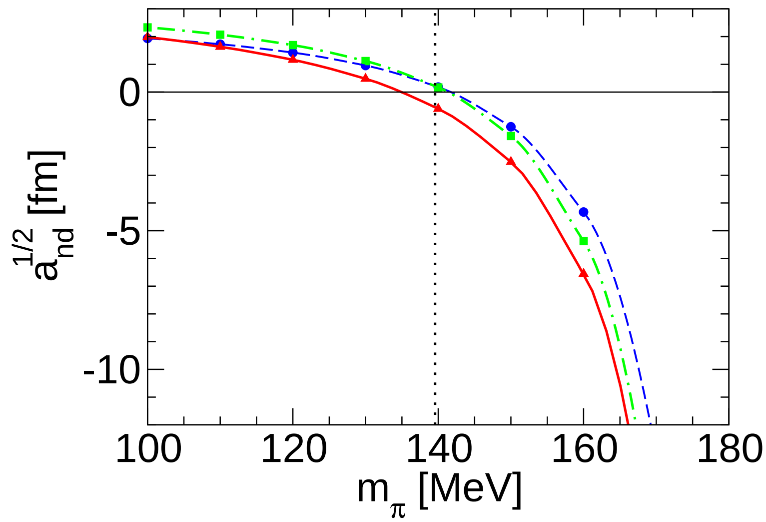

FIG. 7: Doublet neutron-deuteron scattering length $a_{nd}^{1/2}$ around the physical pion mass at LO (dashed), NLO (dash-dotted) and N^{2}LO (solid). Our results have been connected with splines to guide the eye. The dotted line gives the physical pion mass.

in EFT($\not\pi$) . The scattering length is measured at zero momentum. Since we renormalize to a bound state with binding momentum larger than this we do not anticipate any enhancements of the type encoded in Eq. (25). If one takes into account the binding momentum of the deuteron, one could argue that $a_{nd}^{1/2}$ involves typical momenta of order γ, thus the error in the N^{k}LO EFT($\not\pi$) prediction for $a_{nd}^{1/2}$ (or for the quartet scattering length $a_{nd}^{3/2}$) should be, at worst, $(\gamma r)^{k+1}$. In Fig. 6, we show the doublet scattering length $a_{nd}^{1/2}$ in the critical region. The solid line gives the LO result, while the triangles and circles show the NLO and N^{2}LO results. The dotted lines indicate the pion masses at which $a_{nd}^{1/2}$ diverges because the second and third excited states of the triton appear at the neutron-deuteron threshold. These singularities in $a_{nd}^{1/2}(m_\pi)$ are a clear signature that the limit cycle is approached in the critical region. Fig. 6 shows that, as expected from our scaling arguments, the higher-order corrections to $a_{nd}^{1/2}$ are very small and the NLO and N^{2}LO results lie on top of the LO curve. Considering the specific case of the doublet scattering length at $m_\pi = 190$ MeV, we see that

$$a_{nd}^{1/2}(m_\pi = 190 \text{ MeV}) = (93.18 + 0.80 + 0.14) \text{ fm} . \tag{31}$$

At this pion mass we are able to match EFT($\not\pi$) to $B_3^{(1)}$, and we are also fairly far away from any singular points in the function $a_{nd}^{1/2}(m_\pi)$. Consequently, the EFT($\not\pi$) results follow a natural convergence pattern with the expansion parameter γr, which is ≈ 0.08 at this m_π.

While the Efimov effect leads to dramatic effects around the critical pion mass, the pionless EFT can also be used for a similar analysis in the region between $m_\pi^{phys} = 139$ MeV and the lower edge of the critical region. In this pion-mass domain the triton has no excited states. We have therefore used the χEFT results for the pion-mass dependence of the ground (and only) three-nucleon bound state as the three-body input to our EFT($\not\pi$) computation. We then predict the pion-mass dependence of the doublet neutron-deuteron scattering length $a_{nd}^{1/2}$. In Fig. 7 we display EFT($\not\pi$) results at LO, NLO and N^{2}LO. A couple of points in Fig. 7 are particularly worth noting. First, the convergence pattern of EFT($\not\pi$) for $m_\pi \approx 100$ MeV is a little peculiar, with NLO and N^{2}LO corrections essentially canceling to leave the LO

prediction undisturbed. There is also a cancellation in the NLO correction at $m_\pi = m_\pi^{phys}$, which leaves the NLO shift in $a_{nd}^{1/2}$ there accidentally close to zero. Presumably this occurs because at that point the two types of NLO corrections—one proportional to the binding momentum $\kappa^{(0)}$ and the other proportional to γr, are equal in magnitude but opposite in sign. This is consistent with the observed feature that as $m_\pi \to m_\pi^{crit}$ the convergence pattern of the EFT becomes more natural, because $\kappa^{(0)} r$ corrections begin to dominate the γr ones. A second interesting point is that our results suggest that a small decrease in the quark masses could lead to a sign change in the nd doublet scattering length. Perhaps most important, our N^{2}LO EFT($\not\pi$) computation allows us to make a firm prediction (within the scenario under consideration here): as m_q increases above its "real world" value $a_{nd}^{1/2}$ will decrease monotonically until the first triton excited state appears, something that in the critical-point realization studied in Ref. [33] happens at $m_\pi \approx 190$ MeV.

D. Quartet Scattering Length

With results for $a_{nd}^{(1/2)}(m_\pi)$ in hand it is natural to ask whether EFT($\not\pi$) can be used to say anything about nd scattering in the other channel, the quartet. In this case the integral equation describing the scattering is [18, 49]:

$$K_{3/2}^{(n)}(q,q';E) = \tilde{\mathcal{Z}}(q,q';E) + \mathcal{P}\int_0^\Lambda \mathrm{d}q''\, q''^2 \tilde{\mathcal{Z}}(q,q'';E)\tau_t^{(n)}\left(E - \frac{3q''^2}{4M}\right) K_{3/2}^{(n)}(q'',q';E) \quad (32)$$

where

$$\tilde{\mathcal{Z}}(q,q';E) = \frac{1}{2}\frac{M}{qq'}\log\left(\frac{q^2+qq'+q'^2-ME}{q^2-qq'+q'^2-ME}\right) . \quad (33)$$

The prefactor in Eq. (33) is different from Eq. (16). This crucial difference is a consequence of the spin and isospin coupling in the quartet channel, and it guarantees that the integral equation (32) will yield cutoff-independent results without a subtraction being necessary. This is a manifestation of the Pauli principle in this channel, which precludes the appearance of a three-body force without derivatives. In consequence once $\tau_t^{(n)}$ is defined Eq. (32) is straightforward to solve. Up to N^{4}LO the result for $a_{nd}^{3/2}$ is purely a function of γ_t and r_t. Performing LO ($n=0$) and NLO ($n=1$) computations using Eq. (32), and then expanding the NLO result in Taylor series about $r_t = 0$, yields the result for this function:

$$a_{nd}^{3/2} = 1.1791\,\gamma_t^{-1} + 0.5540(6)\,r_t + \mathcal{O}\left(\gamma_t r_t^2\right) . \quad (34)$$

(For N^{2}LO computations of this observable at the physical γ_t and r_t see Refs. [18, 50].) Here the leading-order coefficient of 1.1791 (accurate to the number of digits written) was already obtained in Ref. [49]. The computation of the next-to-leading order coefficient (which has an error of 6 in the last digit) agrees with results from Efimov [51]. The result (34) translates into the results presented in Fig. 8 for $a_{nd}^{3/2}(m_\pi)$. Numerically we have, at the physical pion mass,

$$a_{nd}^{3/2} = 5.0911 \times (1 + 0.190 \pm 0.139)\ \text{fm} = (6.06 \pm 0.71)\ \text{fm}, \quad (35)$$

which is consistent with the experimental value of 6.35 ± 0.02 fm for this quantity [52]. Indeed, the NLO calculation performed here agrees with the experimental number at the 5% level, which is better than expected from our naive-dimensional-analysis estimate of the

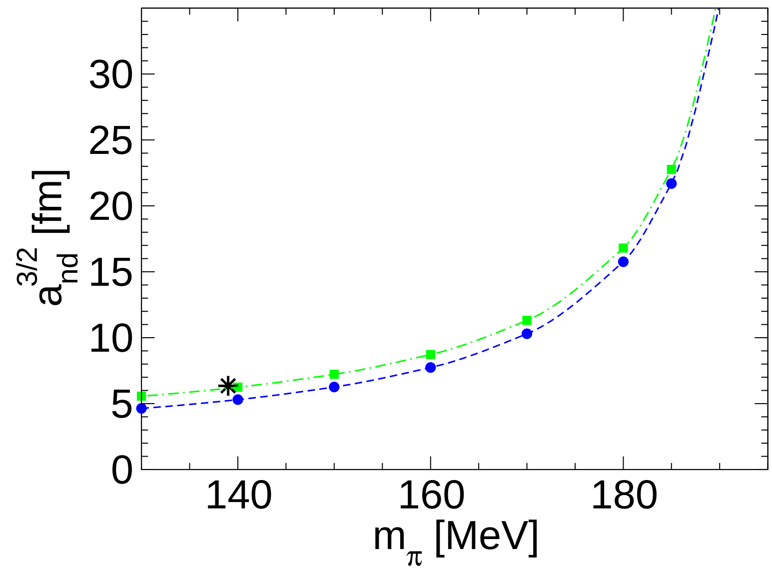

FIG. 8: Quartet neutron-deuteron scattering length $a_{nd}^{3/2}$ around the physical pion mass at LO (dashed) and NLO (dot-dashed). The data points have been connected with splines to guide the eye. The dotted line gives the physical pion mass. The star indicates the experimental value, with the error bar contained within the symbol.

size of the N^{2}LO correction. The accuracy of the EFT($\not\pi$) prediction for $a_{nd}^{3/2}(m_\pi)$ should only improve as we move from the physical pion mass towards m_π^{crit}. Note that once $m_\pi > m_\pi^{crit}$ the quantity $a_{nd}^{3/2}$ cannot be defined, since the spin-1 NN state becomes unbound, and the spin-0 bound state obviously cannot be used to produce a total spin of 3/2.

V. SUMMARY & CONCLUSION

In this paper, we have presented a detailed study of the pion-mass dependence of three-nucleon observables around the critical pion mass and around the physical pion mass. We have performed calculations to N^{2}LO in EFT($\not\pi$) using the pion-mass dependence of the two-nucleon effective range parameters and one triton state from a NLO calculation in χEFT as input.

In particular, we analyzed the convergence pattern of the effective-range corrections at NLO and N^{2}LO in the critical region where $\gamma_s \approx \gamma_t \approx 0$. We found that the convergence of the EFT expansion is slow for the triton ground state but rapid for all remaining states in the three-nucleon Efimov spectrum. This behavior is expected, since the higher-order corrections in the critical region scale with powers of κr, where κ denotes the typical momentum scale of the observable under consideration. Our results demonstrate that the pionless EFT is well suited to describe low-energy observables in few-body systems with a large scattering length. For the triton ground state, it appears to be worthwhile to extend current pionless EFT calculations to N^{3}LO, so as to further investigate the convergence pattern. For the triton excited states in the critical region, the N^{3}LO corrections will be tiny. Although an N^{3}LO calculation would require the inclusion of an additional three-body parameter, the binding energy of the three-nucleon ground state could be calculated if this parameter was matched to scattering data or an excited three-body state.

Directly at the critical pion mass, we have performed a detailed comparison with the triton energies from χEFT. In the zero-range limit, the three-body system displays an exact discrete scale invariance and the ratio of energies of two subsequent Efimov states is $B_3^{(n)}/B_3^{(n+1)} \equiv \exp(2\pi/s_0) \approx 515.03...$. For finite effective range, r, there are corrections to this number proportional to $\kappa^{(n)}r$, where $\kappa^{(n)} \sim (MB_3^{(n)})^{1/2}$ is the binding energy of the nth excited state. However, the exact ratio $\exp(2\pi/s_0)$ is approached as $n \to \infty$ since $\kappa^{(n)} \to 0$ in this limit. For the ratio of the energies of the first and second excited state, we find $B_3^{(1)}/B_3^{(2)} = 514.8$ when the range corrections are included to N^{2}LO. The apparent disagreement of this result with the direct calculation using the χEFT potential [33] was resolved by taking the reduced accuracy for the excited states in that calculation into account [48]. In the simpler pionless EFT, the excited states can be calculated to very high accuracy without much computational effort and the higher-order corrections are small. For the more deeply bound states on the other hand, the convergence of the pionless EFT is slow and high accuracy is possible in χEFT. This calculation provides a prime example of how χEFT and EFT($\not\pi$) complement each other very well.

We have also studied the pion-mass dependence of three-nucleon scattering observables. Directly at the physical pion mass, the nd doublet scattering length $a_{nd}^{1/2}$ is unnaturally small. As a consequence, small variations in the pion mass lead to significant changes in $a_{nd}^{1/2}$. As the pion mass is increased towards the critical value $a_{nd}^{1/2}$ becomes very large and negative, jumping to positive infinity when the first excited state of the triton appears. This behavior repeats as one moves closer to the critical trajectory and more and more excited states of the triton appear. It is a signature of the limit cycle being approached. The source of this strong variation of the doublet scattering length in the critical region is therefore understood and well described by EFT($\not\pi$) . The pion-mass dependence of the nd quartet scattering length at the physical pion mass is much milder. As the critical pion mass is approached, it grows and eventually becomes infinite on the critical trajectory. In contrast to the doublet scattering length, this growth is simply driven by the increase in size of the deuteron and has nothing to do with the limit cycle.

Our results will be useful in the context of future Lattice-QCD calculations of three-nucleon observables. As a first step in this direction, the NN scattering lengths have recently been extracted from NN correlators computed at quark masses corresponding to pion masses between 350 and 590 MeV [1]. Thanks to continuing advances in computer power much progress in this direction can be expected over the next couple of years. Lattice computations of NNN correlators are a high priority since they will provide access to three-nucleon forces directly from QCD, but algorithmic and theoretical advances will be required in order for such calculations to become a reality. One important ingredient in such calculations will be extrapolations of three-nucleon observables as a function of pion mass. In particular, a precise understanding of the behavior of three-nucleon observables in the critical region will be indispensable in making contact with the physical pion mass. In this paper we have investigated the physics involved in such extrapolations and demonstrated the complementarity of χEFT and EFT($\not\pi$) calculations in their development.

Finally, the possible limit cycle in QCD is also very interesting in its own right. First signatures of such a limit cycle have recently been seen in an experiment with cold atoms [53], and it would be interesting to observe a limit cycle in lattice simulations of the three-nucleon system with pion masses around 200 MeV [54]. The pionless effective theory can be understood as an expansion around this limit cycle and will be instrumental in interpreting the lattice results. In this paper, we have demonstrated that the required higher-order

calculations are feasible and converge well.

Acknowledgments

We thank Evgeny Epelbaum for providing us with his results for the pion-mass dependence of the effective ranges and U.-G. Meißner for a careful reading of the manuscript. This work was supported by the Department of Energy under grant DE-FG02-93ER40756, by an Ohio University postdoctoral fellowship, by the EU I3HP "Study of Strongly Interacting Matter" under contract number RII3-CT-2004-506078, by the DFG through funds provided to the SFB/TR 16 "Subnuclear structure of matter", and by the BMBF under contract number 06BN411.

[1] S.R. Beane, P.F. Bedaque, K. Orginos and M.J. Savage, Phys. Rev. Lett. **97**, 012001 (2006) [arXiv:hep-lat/0602010].
[2] V. Bernard and U.-G. Meißner, Ann. Rev. Nucl. Part. Sci. **57**, 33 (2007) [arXiv:hep-ph/0611231].
[3] S. Weinberg, Nucl. Phys. B **363**, 3 (1991); Phys. Lett. B **251**, 288 (1990).
[4] S. R. Beane, P. F. Bedaque, W. C. Haxton, D. R. Phillips, and M. J. Savage, arXiv:nucl-th/0008064.
[5] P. F. Bedaque and U. van Kolck, Ann. Rev. Nucl. Part. Sci. **52**, 339 (2002) [arXiv:nucl-th/0203055].
[6] E. Epelbaum, Prog. Nucl. Part. Phys. **57**, 654 (2006) [arXiv:nucl-th/0509032].
[7] A. Nogga, R.G.E. Timmermans and U. van Kolck, Phys. Rev. C **72**, 054006 (2005) [arXiv:nucl-th/0506005].
[8] M. P. Valderrama and E. R. Arriola, Phys. Rev. C **74**, 054001 (2006) [arXiv:nucl-th/0506047].
[9] M. C. Birse, Phys. Rev. C **74**, 014003 (2006) [arXiv:nucl-th/0507077].
[10] E. Epelbaum and U.-G. Meißner, arXiv:nucl-th/0609037.
[11] J. Mondejar and J. Soto, arXiv:nucl-th/0612051.
[12] S. R. Beane, P. F. Bedaque, M. J. Savage, and U. van Kolck, Nucl. Phys. A **700**, 377 (2002) [arXiv:nucl-th/0104030].
[13] S. R. Beane and M. J. Savage, Nucl. Phys. A **717**, 91 (2003) [arXiv:nucl-th/0208021]; Nucl. Phys. A **713**, 148 (2003) [arXiv:nucl-th/0206113].
[14] E. Epelbaum, U.-G. Meißner, and W. Glöckle, Nucl. Phys. A **714**, 535 (2003) [arXiv:nucl-th/0207089].
[15] E. Braaten and H.-W. Hammer, Phys. Rev. Lett. **91**, 102002 (2003) [arXiv:nucl-th/0303038].
[16] D. B. Kaplan, M. J. Savage and M. B. Wise, Phys. Lett. B **424**, 390 (1998) [arXiv:nucl-th/9801034]; Nucl. Phys. B **534**, 329 (1998) [arXiv:nucl-th/9802075].
[17] U. van Kolck, arXiv:hep-ph/9711222; Nucl. Phys. A **645**, 273 (1999) [arXiv:nucl-th/9808007].
[18] P. F. Bedaque and U. van Kolck, Phys. Lett. B **428**, 221 (1998) [arXiv:nucl-th/9710073]; P. F. Bedaque, H.-W. Hammer and U. van Kolck, Phys. Rev. C **58**, 641 (1998) [arXiv:nucl-th/9802057].
[19] J. Gegelia, Phys. Lett. B **429**, 227 (1998).

[20] M. C. Birse, J. A. McGovern and K. G. Richardson, Phys. Lett. B **464**, 169 (1999) [arXiv:hep-ph/9807302].
[21] E. Braaten and H.-W. Hammer, Phys. Rept. **428**, 259 (2006) [arXiv:cond-mat/0410417].
[22] V. N. Efimov, Sov. J. Nucl. Phys. **12**, 589 (1971).
[23] V. N. Efimov, Sov. J. Nucl. Phys. **29**, 546 (1979).
[24] K. G. Wilson, Phys. Rev. D **3**, 1818 (1971).
[25] V. Efimov, Nucl. Phys. A **362**, 45 (1981).
[26] P. F. Bedaque, H.-W. Hammer, and U. van Kolck, Nucl. Phys. A **676**, 357 (2000) [arXiv:nucl-th/9906032].
[27] V. Efimov and E.G. Tkachenko, Phys. Lett. **157B**, 108 (1985).
[28] H.-W. Hammer and T. Mehen, Phys. Lett. B **516**, 353 (2001) [arXiv:nucl-th/0105072].
[29] P. F. Bedaque, G. Rupak, H. W. Grießhammer and H.-W. Hammer, Nucl. Phys. A **714**, 589 (2003) [arXiv:nucl-th/0207034].
[30] L. Platter and D. R. Phillips, Few Body Syst. **40**, 35 (2006) [arXiv:cond-mat/0604255].
[31] L. Platter, Phys. Rev. C **74**, 037001 (2006) [arXiv:nucl-th/0606006].
[32] H. W. Grießhammer, Nucl. Phys. A **760**, 110 (2005) [arXiv:nucl-th/0502039].
[33] E. Epelbaum, H.-W. Hammer, U.-G. Meißner and A. Nogga, Eur. Phys. J. C **48**, 169 (2006) [arXiv:hep-ph/0602225].
[34] U. van Kolck, Phys. Rev. C **49**, 2932 (1994).
[35] E. Epelbaum, W. Glöckle, and U.-G. Meißner, Nucl. Phys. A **671**, 295 (2000) [arXiv:nucl-th/9910064].
[36] M. R. Schindler, D. Djukanovic, J. Gegelia and S. Scherer, arXiv:hep-ph/0612164.
[37] P. Büttiker and U.-G. Meißner, Nucl. Phys. A **668**, 97 (2000) [arXiv:hep-ph/9908247].
[38] E. Matsinos, arXiv:hep-ph/9807395.
[39] R. A. Arndt, W. J. Briscoe, I. I. Strakovsky and R. L. Workman, Phys. Rev. C **74**, 045205 (2006) [arXiv:nucl-th/0605082].
[40] D. B. Kaplan, M. J. Savage and M. B. Wise, Nucl. Phys. B **478**, 629 (1996) [arXiv:nucl-th/9605002].
[41] C. Ordonez, L. Ray and U. van Kolck, Phys. Rev. C **53**, 2086 (1996) [arXiv:hep-ph/9511380].
[42] N. Kaiser, R. Brockmann and W. Weise, Nucl. Phys. A **625**, 758 (1997) [arXiv:nucl-th/9706045].
[43] E. Epelbaum, private communication (2006).
[44] H.-W. Hammer and T. Mehen, Nucl. Phys. A **690**, 535 (2001) [arXiv:nucl-th/0011024].
[45] I. R. Afnan and D. R. Phillips, Phys. Rev. C **69**, 034010 (2004) [arXiv:nucl-th/0312021].
[46] P. F. Bedaque, H.-W. Hammer, and U. van Kolck, Phys. Rev. Lett. **82**, 463 (1999) [arXiv:nucl-th/9809025]; Nucl. Phys. A **646**, 444 (1999) [arXiv:nucl-th/9811046].
[47] Th. Mehen, I. W. Stewart, and M. B. Wise, Phys. Rev. Lett. **83**, 931 (1999) [arXiv:hep-ph/9902370].
[48] A. Nogga, private communication (2007).
[49] G.V. Skorniakov and K.A. Ter-Martirosian, Sov. Phys. JETP **4**, 648 (1957) [J. Exptl. Theoret. Phys. (U.S.S.R.) **31**, 775 (1956)].
[50] H. W. Grießhammer, Nucl. Phys. A **744**, 192 (2004) [arXiv:nucl-th/0404073].
[51] V. Efimov, Phys. Rev. C **44**, 2303 (1991).
[52] W. Dilg, L. Koester, and W. Nistler, Phys. Lett. **B36**, 208 (1971).
[53] T. Kraemer, M. Mark, P. Waldburger, J.G. Danzl, C. Chin, B. Engeser, A.D. Lange, K. Pilch, A. Jaakkola, H.-C. Nägerl, and R. Grimm, Nature **440**, 315 (2006).

[54] K. G. Wilson, Nucl. Phys. Proc. Suppl. **140**, 3 (2005) [arXiv:hep-lat/0412043].